Electronic Supplementary Information for:

Simulation of Magnetite Nanoparticle Mobility in a Heterogeneous Flow Cell

Bonnie A. Lyon-Marion[1], Matthew D. Becker[1], Anthony A. Kmetz[1†], Edward Foster[2], Keith P. Johnston[2], Linda M. Abriola[1], Kurt D. Pennell[1*]

[1]Department of Civil and Environmental Engineering, Tufts University, Medford, Massachusetts 02155, United States

[2]McKetta Department of Chemical Engineering, The University of Texas at Austin, Austin, Texas 78712, United States

[*]Corresponding author:

Kurt D. Pennell, PhD, PE, BCEE
Department of Civil & Environmental Engineering
Tufts University
200 College Avenue
Medford, MA 02155
Tel: 617-627-3099
Fax: 617-627-3994
Email: kurt.pennell@tufts.edu

[†] Current affiliation: Aramco Services Company: Aramco Research Center - Boston , Cambridge, MA 02139, United States

Table of Contents

Nanoparticle Synthesis

Magnetite nanoparticles (nMag) were synthesized using the procedure described by Urena-Benavides et al.[1] A schematic of the synthesis process is shown in Figure S1 and Figure S2 shows a transmission electron microscopy (TEM) image of the polymer-coated nMag. Figures are reprinted with permission from Urena-Benavides et al.[1] Copyright 2016 American Chemical Society.

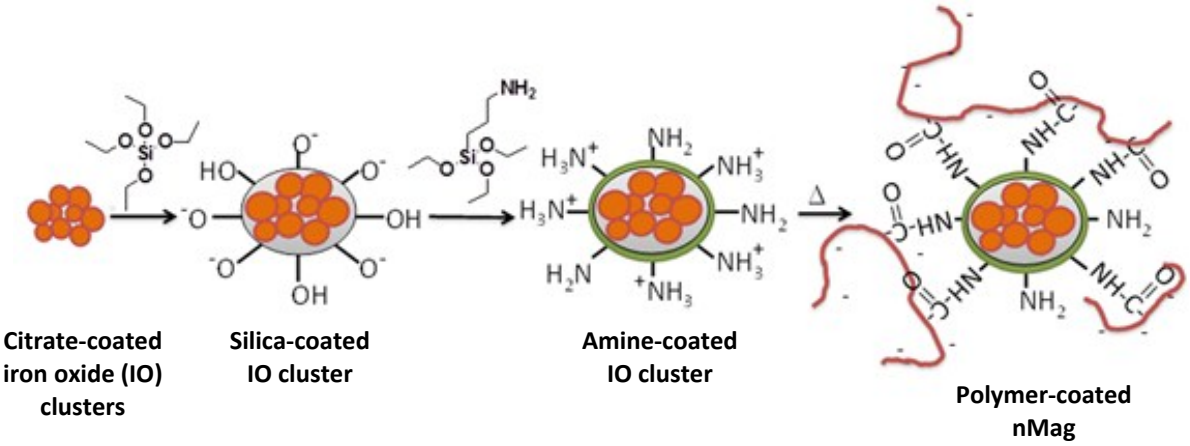

Supplementary Figure S1. Schematic diagram of nMag synthesis procedure.

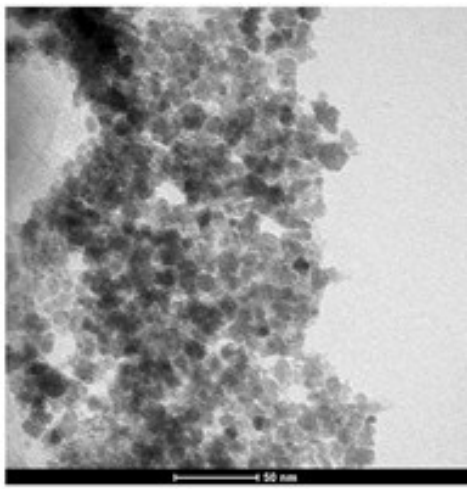

Supplementary Figure S2. TEM image of polymer-coated nMag. Image was obtained using an FEI TECNAI Spirit Bio Twin operated at 80 kV. Scale bar shown at bottom of image represents 50 nm.

Text S1. Analytical Methods

Non-reactive tracer samples from column experiments were diluted by a factor of 50 with deionized (DI) water and measured using a bromide probe (Cole-Parmer North America Vernon Hills, IL). Bromide samples from the flow cell tracer tests were analyzed using a Dionex ICS 2100 ion chromatograph using an AS-18 fast column/AG-18 guard column and 23 mM potassium hydroxide eluent (Thermo Scientific, Waltham, MA). The densities of nMag solutions and brine were measured in triplicate using a 25-mL glass pycnometer. Solid samples were prepared for scanning electron microscopy (SEM) imaging by placing sand grains on conductive double-sided carbon tape attached to an aluminum stub mount (Electron Microscopy Sciences, Hatfield, PA). The solid samples were then air-dried overnight and imaged with a Zeiss Supra55 Variable Pressure field emission SEM (Carl Zeiss Microscopy, Peabody, MA), operated under high vacuum with an SE2 detector and beam voltage of 3 kV. The presence of nMag in SEM samples was confirmed using the spectrum function of an energy dispersive X-ray spectroscopy (EDS) detector attached to the SEM and analyzing for iron content in regions that were interrogated versus not interrogated by nMag.

Text S2. Mathematical Model Development

Simulation of nMag transport in the packed cell required appropriate characterization of the background flow field. The boundary conditions for all sides of the heterogeneous cell were set as no-flow. To model the influent and effluent chambers, the first and last columns of the numerical grid were assigned very high permeability values relative to that of the background coarse sand media. The constant pressure head condition that created flow in the experiment was simulated by assigning a constant hydraulic head to single cells in each of the influent and effluent chambers. The locations of these constant pressure cells were consistent with the heights of the influent and effluent wells located inside the end chambers. All simulations were conducted on a numerical grid with cells that ranged from 0.5 cm × 0.5 cm within the lens and injection regions of the flow cell to 1 cm × 1 cm within the bulk coarse sand regions of the flow cell. Grid sensitivity analyses revealed that this discretization level provided a sufficient level of resolution for the tracer and nanoparticle plume evolution without creating burdensome computational demands.

To incorporate the influence of variable grain size and flow rate (present in the heterogeneous flow cell) on S_{max} in the mathematical model, the approach of Li et al.[2] was employed, where S_{max} values are fit to a power function of the normalized diffusive mass flux of nMag particles to the surface. Figure S2 presents a plot of parameter data and the best fit S_{max} power function:

$$S_{max} = 230.93 * \Lambda^{-0.585}$$

$$\Lambda = Pe^{\frac{1}{3}} * \left(\frac{d_c}{d_M}\right)$$

where Λ is the normalized mass flux of nanoparticles to the solid/liquid interface, d_c is a representative collector size for the porous medium, and d_M is the diameter of a medium grain sand (0.5 mm). The mean diameters of 40-50 and 80-100 mesh Ottawa sand (335 and 165 μm) were used as the d_c for the coarse and fine sand, respectively. Using equations (S1) and (S2), values of S_{max}^{n} obtained from the one-dimensional column experiments can be related to the physical parameters of the system, and thereby applied to larger, multi-dimensional systems with heterogeneous media and flow fields, similar to the approaches used in previous studies.[3-5]

References

1. Ureña-Benavides, E. E.; Lin, E. L.; Foster, E. L.; Xue, Z.; Ortiz, M.; Fei, Y.; Larsen, E. S.; Kmetz, A. A.; Lyon, B. A.; Bielawski, C. W.; Pennell, K. D.; Ellison, C. J.; Johnston, K. P., Low Adsorption of Magnetite Nanoparticles with Uniform Polyelectrolyte Coatings in Concentrated Brine on Model Silica and Sandstone. *Ind. Eng. Chem. Res.* **2016,** *55*, (6), 1522-1532.

2. Li, Y.; Wang, Y.; Pennell, K. D.; Abriola, L. M., Investigation of the Transport and Deposition of Fullerene (C60) Nanoparticles in Quartz Sands under Varying Flow Conditions. *Environ. Sci. Technol.* **2008,** *42*, (19), 7174-7180.

3. Cullen, E.; O'Carroll, D. M.; Yanful, E. K.; Sleep, B., Simulation of the subsurface mobility of carbon nanoparticles at the field scale. *Adv. Water Resour.* **2010,** *33*, 361-371.

4. Bai, C.; Li, Y., Modeling the Transport and Retention of nC_{60} Nanoparticles in the Subsurface under Different Release Scenarios. *J. Contam. Hydrol.* **2012,** *136-137*, 43-55.

5. Bai, C.; Li, Y., Time series analysis of contaminant transport in the subsurface: Applications to conservative tracer and engineered nanomaterials. *J. Contam. Hydrol.* **2014,** *164*, 153-62.

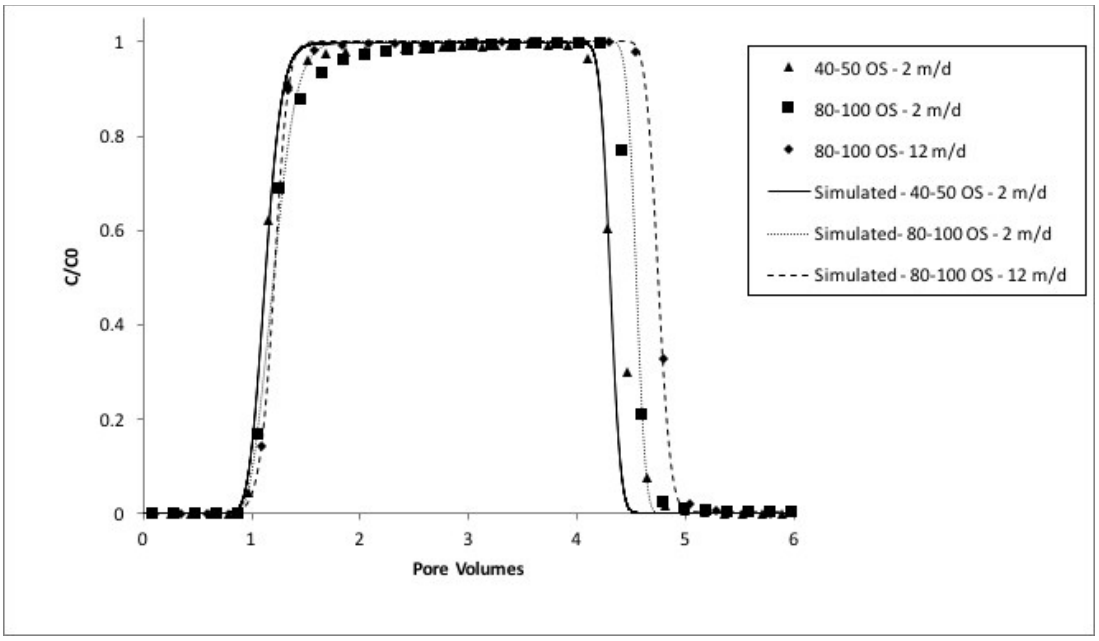

Supplementary Figure S3. nMag transport through 40-50 and 80-100 mesh Ottawa sand columns run at 2 m/day seepage velocity and 80-100 Ottawa sand at 12 m/day seepage velocity. Symbols represent experimental measurements and solid lines indicate model fits for parameterization.

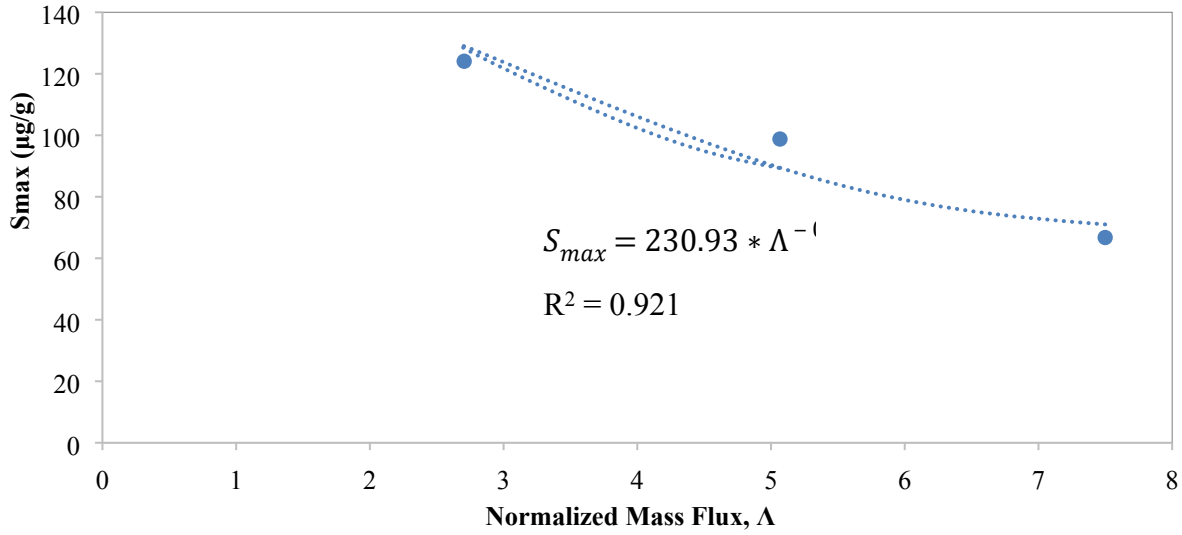

Supplementary Figure S4. Fitted S_{max} relationship with normalized mass flux, $\Lambda = Pe^{\frac{1}{3}} * \left(\frac{d_c}{d_M}\right)$. Here, solid circles represent S_{max} values obtained from individual column experiments, and the dotted line represents the best fit power function (equation (S1)).

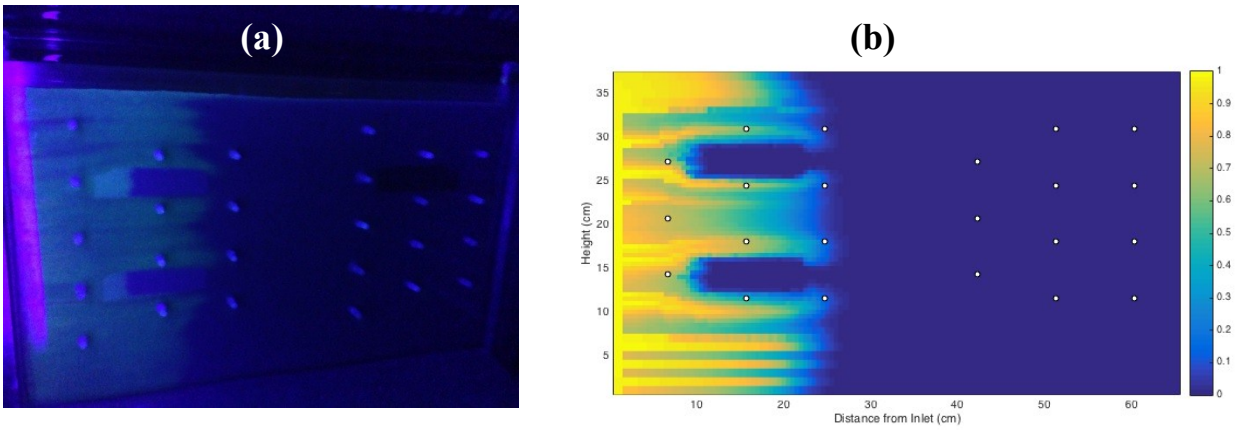

Supplementary Figure S5. (a) Observed and (b) simulated non-reactive tracer (fluorescein) at time = 173 min after start of influent tracer injection. Color bar in (b) represents normalized concentration (C/C_0).

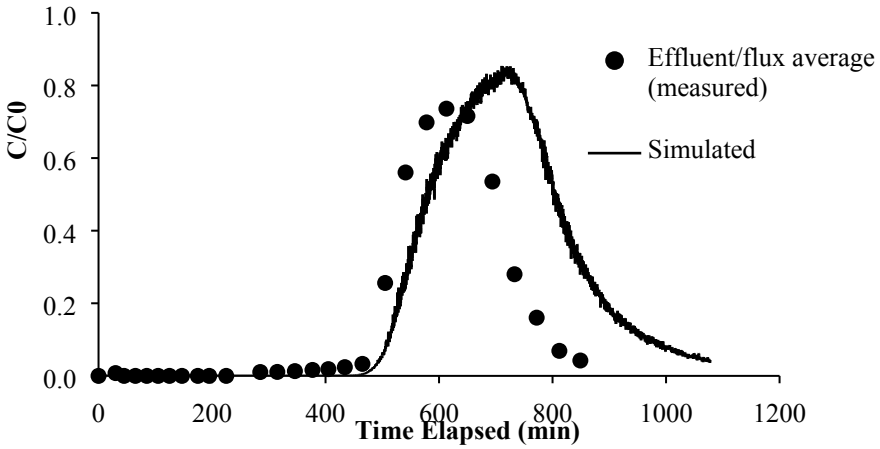

Supplementary Figure S6. Measured and simulated non-reactive tracer (bromide) breakthrough curve (BTC) for flow cell effluent (flux average) samples collected during influent tracer experiment.

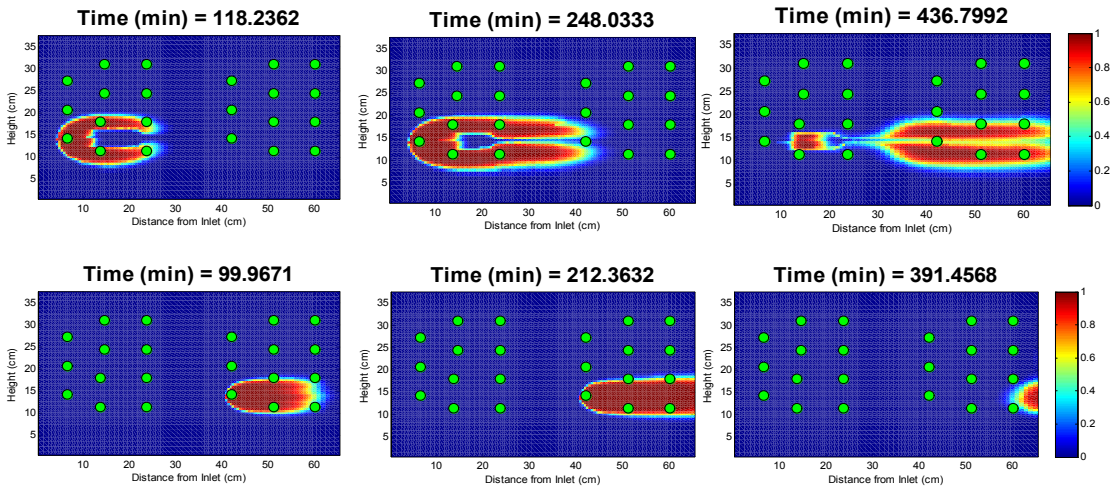

Supplementary Figure S7. Simulated tracer injections in A4 injection port upstream of fine sand lens (top row) and D4 injection port upstream of course sand background (no lens) (bottom row). Color bar represents normalized concentration (C/C_0).

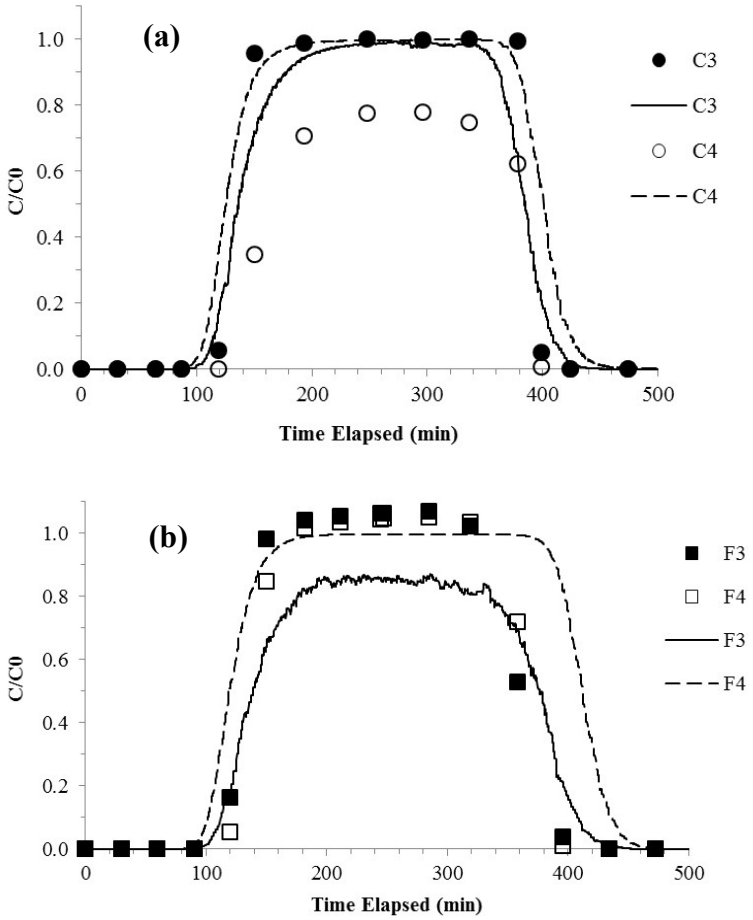

Supplementary Figure S8. Measured and simulated non-reactive tracer (bromide) BTCs from samples collected following tracer injection into port (a) A4 (80-100 mesh Ottawa sand lens) and (b) D4 (control, no lens). Sampling ports correspond to letter/number shown in Figure 1.

Supplementary Table S1. 2.5D Flow cell nanoparticle injection parameters.

Experiment	Injection port	nMag conc. (mg/L)	Injected volume (mL)	Injection rate (mL/min)	nMag diameter* (nm)	Downstream ports sampled
Control (no lens)	D4	2584	203	0.75	189±4.0	E3, E4, F3, F4
Fine sand lens	A4	2874	203	0.75	181±2.4	B3, B4, C3, C4, D5, E4

*Z-average size measured by DLS, value represents average between triplicate samples at start and end of injection ± standard deviation (*n*=6)

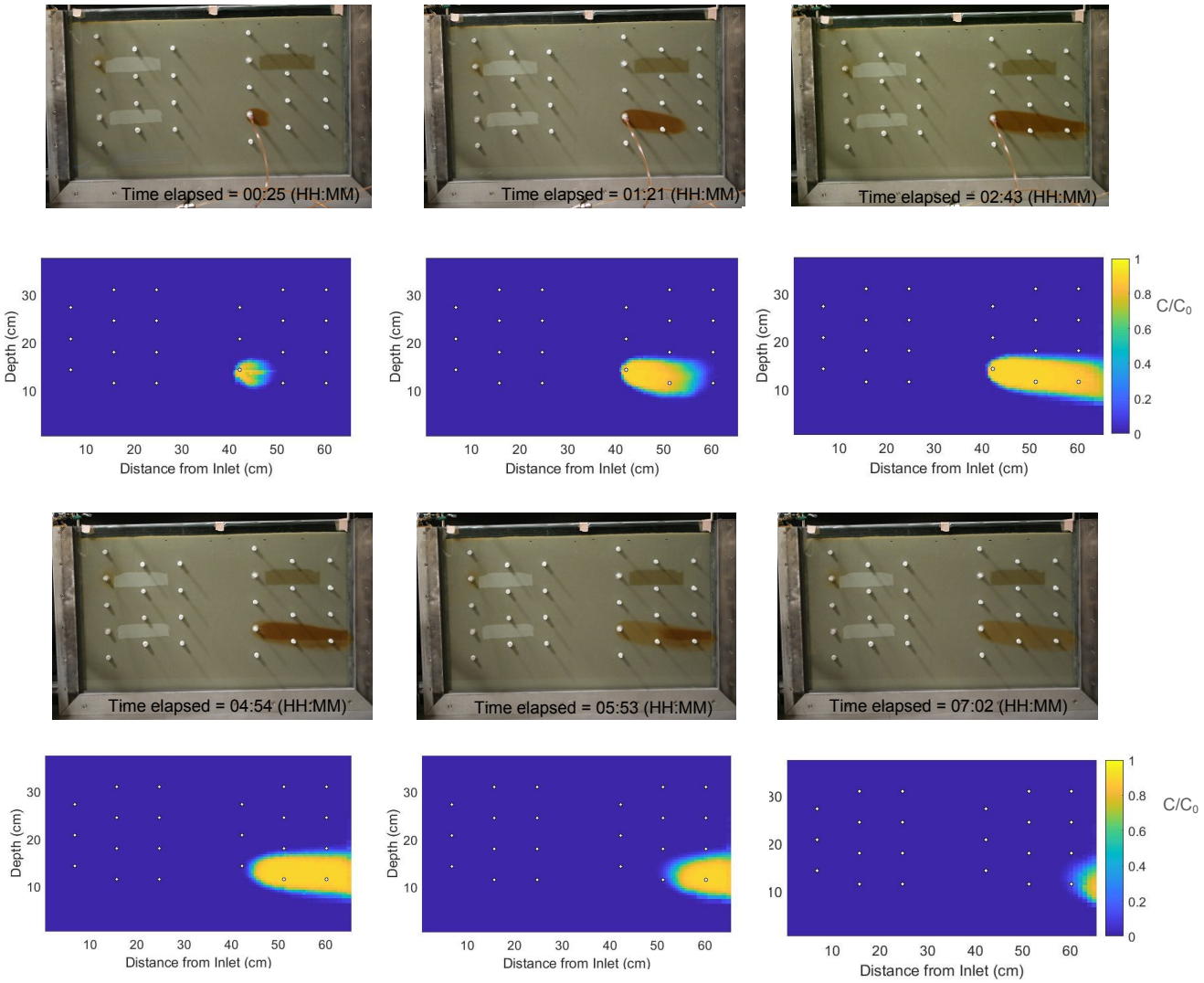

Supplementary Figure S9. Observed and predicted nMag transport through control (no lens) injection. Time elapsed since start of injection is shown in minutes.

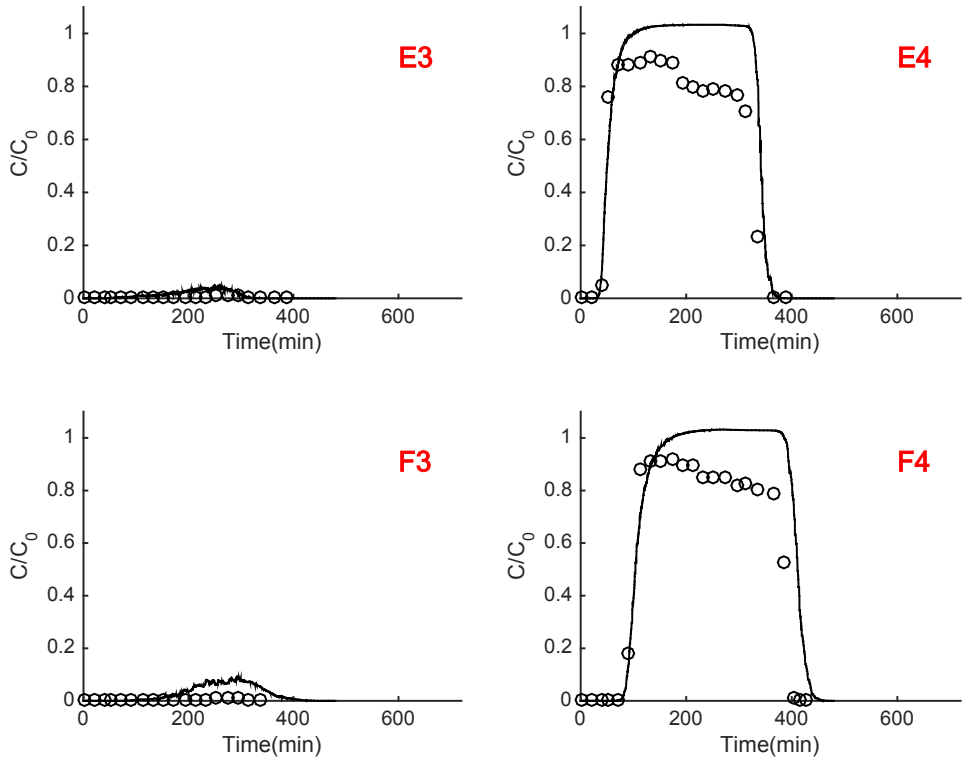

Supplementary Figure S10. Measured (open circles) compared to predicted (solid line) nMag effluent concentrations for control (no lens) injection. Port location is noted in top right of each figure.

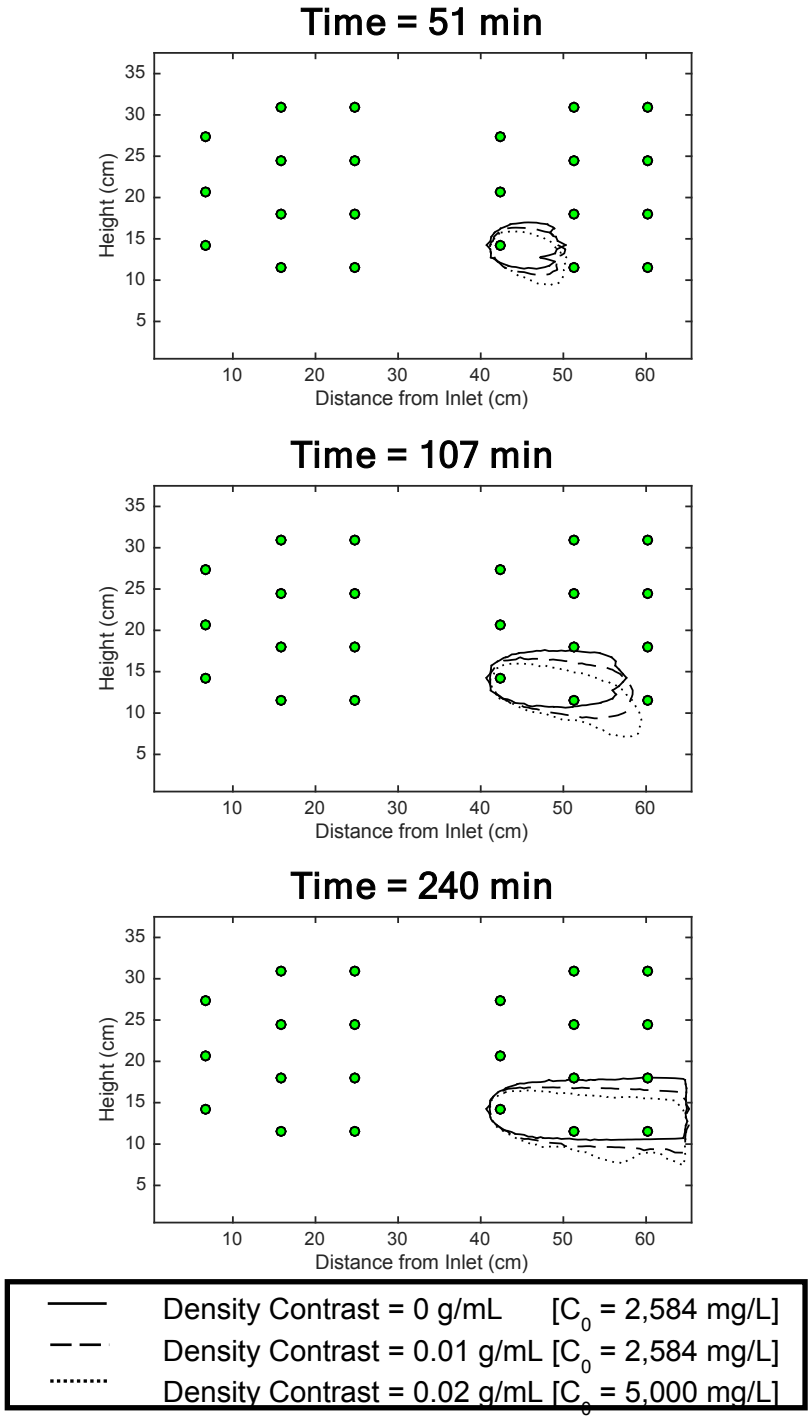

Supplementary Figure S11. Impact of density contrast between injected nanoparticle suspension and background electrolyte on two-dimensional nanoparticle transport. Contours represent the boundary of $C/C_0 = 0.8$. Note that all simulations considered nanoparticle transport and solid-phase attachment. The 'Density Contrast = 0 g/mL' case was simulated by neglecting the influence of nMag concentration on injection fluid density.

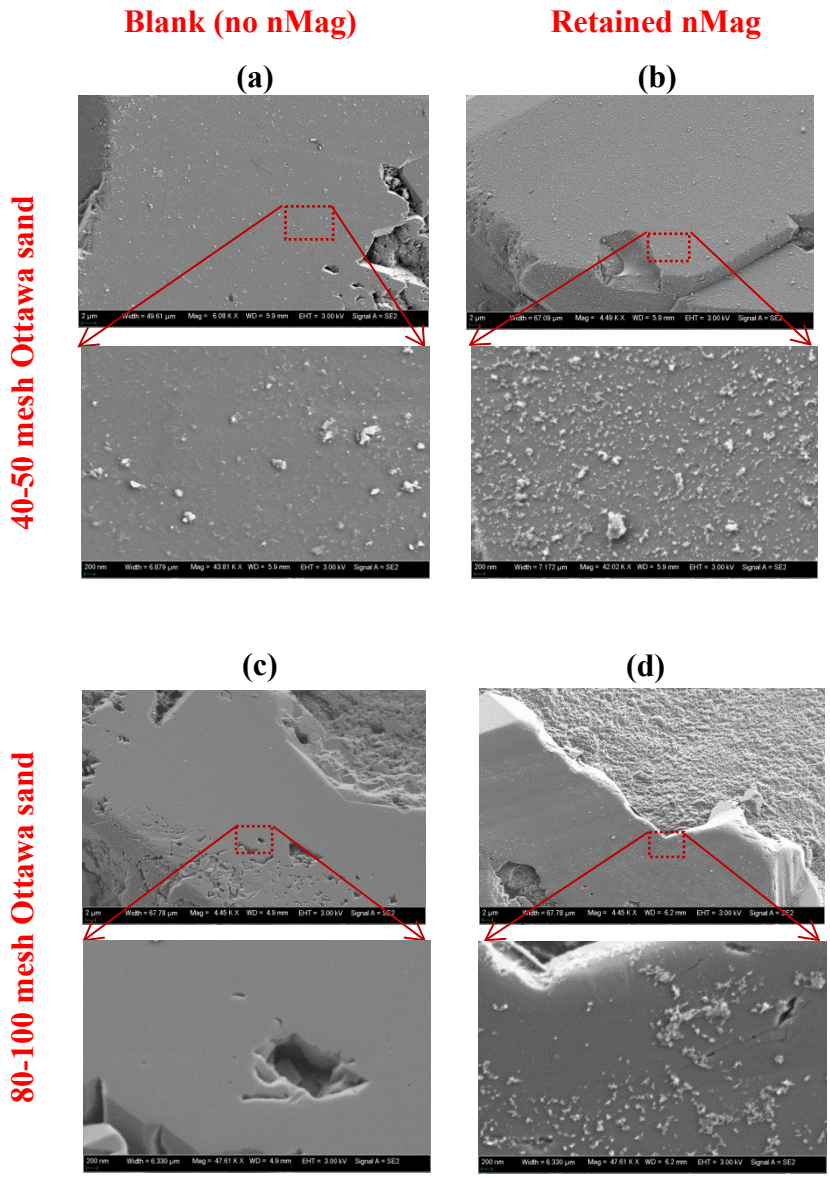

Supplementary Figure S12. SEM images of blank (a) unwashed 40-50 mesh Ottawa sand, (c) washed 80-100 mesh Ottawa sand, and nMag retained on (b) unwashed 40-50 mesh Ottawa sand, (d) washed 80-100 mesh Ottawa sand. Insets show increasing magnification with scale bar shown in lower left corner of each image.

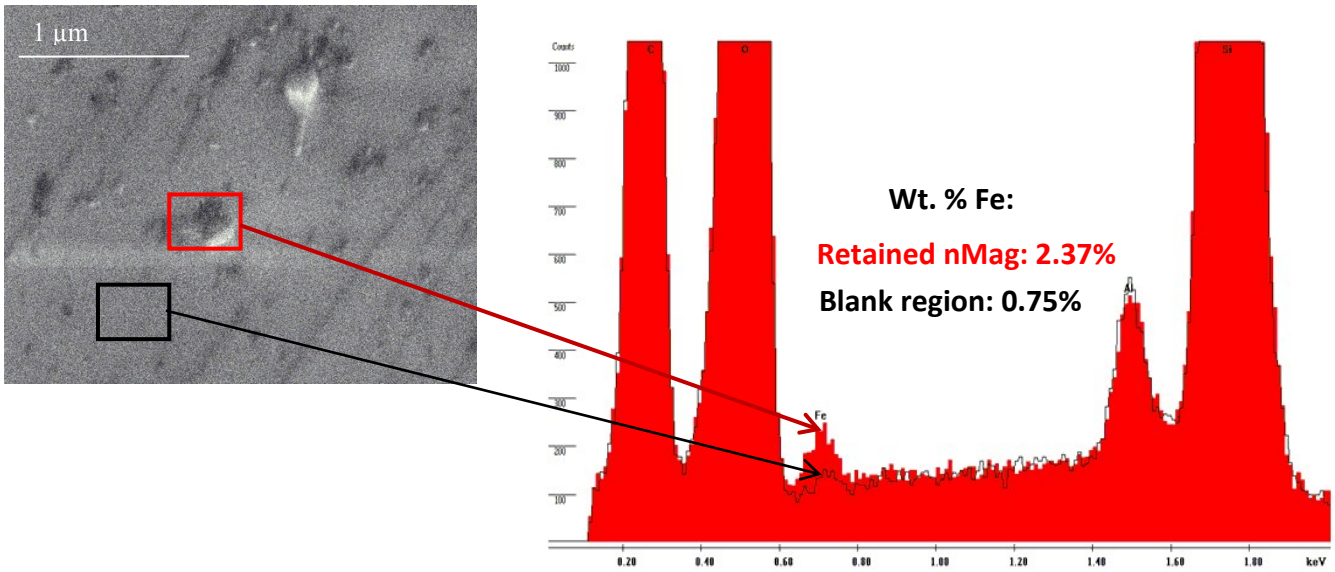

Supplementary Figure S13. Energy dispersive x-ray spectroscopy (EDS) spectrum of nMag attached to Ottawa Sand (red) overlain with blank Ottawa sand spectrum (black line) obtained using a Supra55VP field emission scanning electron microscope (SEM) in variable pressure mode, EHT voltage = 10 kV.